Polymer 49 (2008) 3892–3901

Contents lists available at ScienceDirect

Polymer

journal homepage: www.elsevier.com/locate/polymer

Using steered molecular dynamics simulations and single-molecule force spectroscopy to guide the rational design of biomimetic modular polymeric materials

Dora L. Guzmán [a], Jason T. Roland [a], Harindar Keer [a], Yen Peng Kong [c], Thorsten Ritz [b,*], Albert Yee [c,*], Zhibin Guan [a,*]

[a] Department of Chemistry, University of California, 1102 Natural Sciences 2, Irvine, CA 92697-2025, United States
[b] Department of Physics, University of California, 4129 Frederick Reines Hall, Irvine, CA 92697-4575, United States
[c] Department of Chemical Engineering and Materials Science, University of California, 916 Engineering Tower, Irvine, CA 92697-2575, United States

ARTICLE INFO

Article history:
Received 13 March 2008
Received in revised form 26 June 2008
Accepted 27 June 2008
Available online 3 July 2008

Keywords:
Steered molecular dynamics (SMD)
Single-molecule force spectroscopy (SMFS)
Atomic force microscope (AFM)

ABSTRACT

This article describes results on using steered molecular dynamics (SMD) simulations and experimental single-molecule force spectroscopy (SMFS) to investigate the relationship between hydrogen bonding and mechanical stability of a series of homodimeric β-sheet mimics. The dimers consisting of 4, 6, and 8 H-bonding sites were modeled in explicit chloroform solvent and the rupture force was studied using constant velocity SMD. The role of solvent structuring on the conformation of the dimers was analyzed and showed no significant contribution of chloroform molecules in the rupture event. The simulated stability of the dimers was validated by force data obtained with atomic force microscopy (AFM)-based SMFS in toluene. The computational model for the 8H dimer also offered insight into a possible mismatched dimer intermediate that may contribute to the lower than expected mechanical stability observed by single-molecule AFM force studies. In addition, atomic level analysis of the rupture mechanism verified the dependence of mechanical strength on pulling trajectory due to the directional nature of chemical bonding under an applied force. The knowledge gained from this basic study will be used to guide further design of modular polymers having folded nanostructures through strategic programming of weak, non-covalent interactions into polymer backbones.

Published by Elsevier Ltd.

1. Introduction

Nature has provided a myriad of biopolymers that exhibit remarkable and highly specific mechanical responses to external stress. Understanding the mechanism by which nature has evolved such materials is of great interest to materials scientists. The field of synthetic biology, or biomimetics, strives to harness this knowledge and reapply it to new materials design for technological applications. The advent of the atomic force microscope made possible mechanical manipulation of single molecules that sequentially unfold domains through an applied force across their termini [1,2]. This powerful technique has provided crucial information about the nanomechanical properties of such materials. The most comprehensively studied of these mechanical proteins is the skeletal muscle protein titin, which gives muscle its elastic properties via a passive force mechanism [3–5]. Comprised of approximately 300 homologous immunoglobulin (Ig) domains tethered in a linear array, the protein responds selectively to an external stress. Single-molecule force spectroscopy studies revealed a characteristic saw tooth pattern originating from sequential unfolding of its unique modular multi-domain structure [3]. This method of sacrificial bond rupture of hierarchical architectures appears to be a general mechanism used in nature to achieve advanced material properties. Application of these concepts in the design of synthetic materials has remained a challenge in materials science.

To gain insight into the molecular mechanisms giving rise to the mechanical function observed in titin domains, Schulten et al. conducted computational SMFS, or SMD simulations, designed to closely mimic experimental single-molecule force spectroscopy studies, where one terminus is fixed in space (i.e. substrate) and the other is restrained to a harmonic spring (i.e. force probe) moving with constant velocity in a given direction. The original work by Schulten demonstrated the importance of shearing mechanical bonds in natural domains to enhance mechanical stability [6]. SMD simulations of the titin I27 domain also identified 9 strategic interstrand hydrogen bonds involved in the unfolding against an

* Corresponding authors. Tel.: +1 949 824 5172; fax: +1 949 824 2210.
E-mail address: zguan@uci.edu (Z. Guan).

0032-3861/$ – see front matter Published by Elsevier Ltd.
doi:10.1016/j.polymer.2008.06.047

applied force [5]. At low forces three hydrogen bonds rupture, forming an intermediate observed as a hump in single-molecule force-extension curves that deviate from the model of entropic elasticity (worm-like chain). At higher forces simultaneous rupture of 6 sacrificial bonds precedes the rapid unfolding of the entire domain. The intermediate identified in the simulations was experimentally verified by disrupting the hydrogen bonds through protein engineering, eliminating the observed deviation [5]. Additionally, Li et al. verified the mechanical strength derived from the 6 hydrogen bonds through proline mutation of the residues involved, leading to altered mechanical stability [7].

Inspired by this modular concept for rational materials design, our group has demonstrated that the modular elongation mechanism can be employed for synthetic polymers in organic solvents to increase their overall strength and toughness by incorporating strong and precise hydrogen bonding motifs into the polymer backbone [8–10]. Single-molecule force studies of the polymer showed the characteristic saw tooth pattern from unfolding of loops as the polymer was stretched. Bulk stress–strain measurements demonstrated that the modular polymer combines high tensile strength, high toughness, and elasticity. Although the polymers in our previous studies exhibited enhanced mechanical properties [8–10], the tunability of the system was limited due to the predetermined quadruple H-bonded ureido-4[1*H*]-pyrimidinone (UPy) structure. To overcome this limitation, our current study analyzes a series of peptidomimetic β-sheets designed to allow the thermodynamic stability of the hydrogen-bonded homodimers to be varied systematically by choosing the length and sequence of the hydrogen-bonded array (Fig. 1). The application of SMD to reveal the molecular mechanisms underlying the mechanical properties of various biomolecules [11–13], prompted us to use modeling to investigate the atomic level detail of our synthetic modular building blocks. This article describes our efforts in incorporating SMD simulations as a tool to aid in the design of novel materials with advanced mechanical properties. Such computational models can enhance our understanding on the relationship between the cooperative effect of weak molecular interactions and mechanical stability, and further predict the mechanical properties of novel systems.

To explore the structure–property correlation, we constructed a series of well-defined peptidomimetic β-sheets initially designed by Gong and coworkers consisting of donor (D) and acceptor (A) units containing 4 (DADA, **1**), 6 (AADADD, **2**), and 8 (AADADADD, **3**) H-bonding sites, respectively (Fig. 1, see Supplementary data for detailed description on synthesis and characterization) [14]. The sequences were designed to minimize other possible dimerization modes. Unlike most proteins, the peptidomimetic β-sheet structures are not soluble in water, and therefore, were investigated in organic solvents (i.e. chloroform and toluene). It should be emphasized that the focus of this study is to gain fundamental understanding on the relationship between hydrogen-bonded nanostructures and their nanomechanical properties, which will aid us designing polymeric materials with superior mechanical properties. For many applications of polymers, the bulk phases of the polymers are exposed to a hydrophobic environment. Therefore, the information obtained in non-polar organic solvents is highly relevant to the final material's design. The thermodynamic dimerization constants for the 4 and 6 H-bonding systems were reported to be approximately $4 \times 10^4\ M^{-1}$ and $6 \times 10^9\ M^{-1}$, respectively; and the system with 8 H-bonds has a K_d that is too high to measure by conventional methods [14]. In our studies, we first applied SMD to investigate the detailed unfolding trajectory and the dependence of mechanical unfolding force on the number of H-bonds. Following computational modeling, we further carried out AFM–SMFS to validate the computational results. Through a combination of computational and experimental SMFS, we attempted to gain detailed structure–property information to guide our design of new biomimetic polymeric materials with superior mechanical properties.

2. Molecular dynamics methods

2.1. System preparation: topology and parameterization

All simulations were performed using the software package NAMD [15] with the all-atom CHARMM [16] force field. The visual molecular dynamics (VMD) [17] program version 1.8.5 was used to prepare input files and analyze output trajectories. Because the original CHARMM parameter files do not contain the force

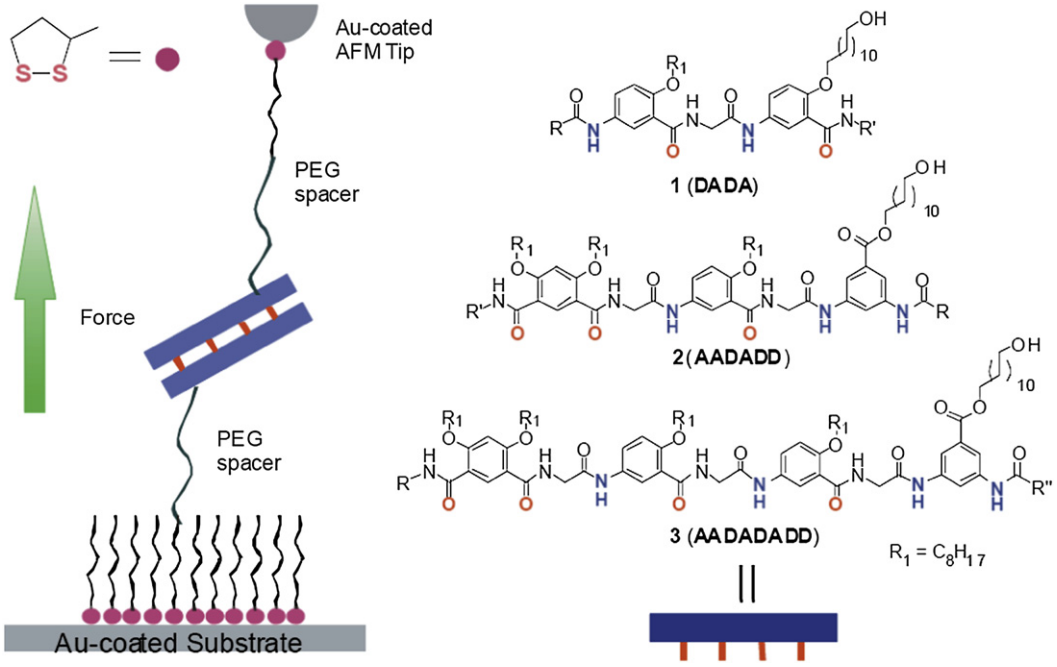

Fig. 1. Left: schematic representation of SMFS studies using AFM; right: structures of the 4H, 6H, and 8H peptidomimetic β-sheets used in this study.

constants for the exact atom types in the synthetic dimers, we estimated the bonding, van der Waals, and partial charges by analogy using similar groups in the CHARMM27 force field database following MacKerell's method [18]. The chloroform solvent model was taken from the AMBER [19] force field, which was verified to yield the correct macroscopic parameters for chloroform within the CHARMM force field. All corresponding topology and parameter files used in these calculations are available upon request.

2.2. Minimization and equilibration of dimer models

Initial dimer coordinates were generated with the program Macromodel using NMR structural analysis data obtained for the peptidomimetic β-sheets in solution (see Supplementary data). The SOLVATE plugin of VMD was modified to include the chloroform box and used to immerse the dimers in the solvent. The size of the systems varied from 25,000 to 38,000 atoms, depending on the molecular surface of the dimers. This ensured complete solvation of the strands even after full dimer dissociation. The resulting system was energy-minimized for 10,000 steps, and subsequently heated to 300 K and equilibrated for over 1 ns prior to performing SMD simulations. The simulations were conducted with a time step of 1 fs for integration of Newton's equations, and a cutoff of Coulomb forces with a switching function starting at 10 Å and reaching zero at 13 Å. Simulations were carried out in the *NVT* ensemble, with constant temperature maintained by using Langevin dynamics. The calculations used full electrostatics with Particle–Mesh–Ewald (PME) summation and periodic boundary conditions (PBC) to eliminate surface effects from the computation.

2.3. Steered molecular dynamics studies

SMD simulations were carried out as described by Schulten and Lu [6] with constant velocity stretching by fixing one terminus of the dimer (red atom) and applying an external force to the other terminus (blue atom) (Fig. 2). A virtual harmonic spring attached to the blue atom is pulled at constant velocity v in the desired direction. The force probed by the virtual spring can be calculated using $F = k(vt - (x_0 - x))$, where $k = 416$ pN/Å, v is the velocity, t is time, and x and x_0 are the positions of the blue atom and the spring's opposite end, respectively. The simulations were performed at 300 K in explicit chloroform solvent using constant velocities of 0.01, 0.1, 0.5, and 1.0 Å/ps.

3. SMFS studies by atomic force microscopy (AFM)

3.1. Modification of gold-coated silicon wafers and AFM cantilever tips

Silicon wafers (4 cm) were coated with a 100 Å thick chromium adhesion layer followed by a 1000 Å layer of gold via electron beam vapor deposition. The gold wafer was cut into 1 cm × 1 cm squares and individual squares were cleaned in piranha solution, washed thoroughly with nanopure H_2O and filtered acetone, and dried under a stream of nitrogen (extreme care should be used when working with piranha solution; piranha may explode without warning!). The gold substrate and gold-coated AFM cantilevers (Asylum Research TR400PB) were submerged into a 4 mM solution of lipoic acid-functionalized PEG in filtered chloroform for 24 h. The samples were removed and carefully rinsed with filtered chloroform by a short incubation in a vial containing pure chloroform. The substrate and cantilever tips were dried under a stream of nitrogen and used immediately for β-sheet mimic functionalization.

3.2. Functionalization of PEG monolayers with β-sheet mimics

Deprotected β-sheet alcohols **1**–**3** (Fig. 1) were dissolved in chloroform (final concentration of 0.1 M) and treated with 5 equivalents of 1,6-diisocyanatohexane (HDI). One drop of dibutyltindilaurate (DBTDL) was added to serve as the catalyst for the reaction between the isocyanate and hydroxyl functionalities to form urethane. After 6 h the starting material had been consumed. The solvent was removed *in vacuo* and the crude material was washed with anhydrous hexane to remove the unreacted HDI. The crude material was diluted to 1 mM in anhydrous chloroform and filtered through a 0.2 μm filter. The clean, dry PEG monolayers (on gold-coated silicon and gold-coated AFM cantilevers) were submerged into the filtered 1.0 mM solution of isocyanate-terminated β-sheet mimic. One drop of DBTDL was again added as the catalyst. After 24 h the cantilevers and substrates were removed, washed with pure chloroform and submerged in toluene for immediate use in AFM single-molecule force spectroscopy.

3.3. AFM single-molecule force spectroscopy

AFM–SMFS was performed on a NT-MDT NTegra AFM running a customized NOVA SPM software package. Experiments were carried out with a universal SPM head (NT-MDT SF005NTF) and an X, Y, and Z closed loop sample scanner (NT-MDT SC250NTF). All samples were probed in toluene using an open liquid cell (NT-MDT AU028). Samples were probed using Asylum Research TR400PB cantilevers. Force experiments were run by selecting a 5 μm × 5 μm square on the sample and running pulling experiments (200 nm/s) at 2500 different points (50 point × 50 point grid).

4. Results and discussion

4.1. Analysis of solvation effects

Prior to performing simulated force studies, we investigated the effects of solvation of the 6H peptidomimetic β-sheet in chloroform using the VMD software. In contrast to proteins where water

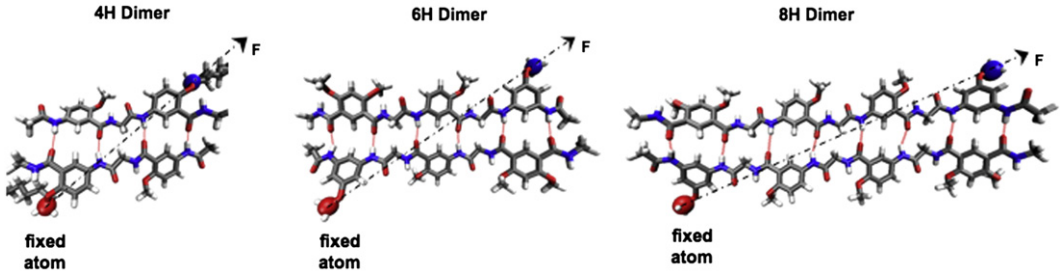

Fig. 2. Peptidomimetic β-sheet model structures depicting the atoms involved in SMD; red atoms were fixed during the simulations, while the blue atoms were harmonically restrained to a virtual spring and pulled in the direction of the force vector (black arrow). Graphics were generated using VMD. (For interpretation of the references to colour in this figure legend, the reader is referred to the web version of this article.)

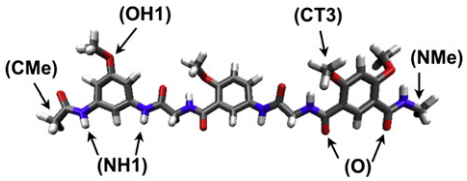

Fig. 3. Selected atom types on the 6H peptidomimetic monomer.

molecules have been shown to facilitate the bond rupture process through competitive hydrogen bonding [20], it was not expected that the relatively non-polar chloroform molecules would have the same effect on the dimers. Previous MD simulations have demonstrated that solvation of chloroform to acetyl residues is weak and dynamic, rapidly exchanging solvent molecules at the solvation site [21]. We analyzed the structured chloroform molecules with radial distribution functions, $g(r)$, around the various atom types of oxygen, nitrogen, and methyl groups of the peptidomimetic dimer (Fig. 3). The radial distribution function (RDF) provides the probability of finding a pair interaction within a given distance r. Characteristic features of the first solvation shell of chloroform molecules around specified sites on the bound 6H dimer and the dissociated strands after bond rupture are shown in Fig. 4.

The RDF results showed overall weak association of the chloroform molecules around the peptidomimetic dimer. The bound dimer strands were first investigated with various combinations of the chloroform molecules with selected atom types (Fig. 4A). The major solvation peaks were observed at a radius of 2.4 Å between the chlorine hydrogen atoms (HX) and carbonyl (O) and ether (OH1) oxygen atoms of the dimer. However, the peak intensities were only between 1.4 and 1.7, indicating weak solvent structuring around the dimer. The second major peaks at approximately 4 Å pertain to the chloride atoms of chloroform (Cl) and the amide methyl (NMe), acetyl methyl (CMe), and the ether methyl (CT3) groups of the dimer. As expected, the intensities of these peaks were all below 1.5, showing no significant organization.

Solvent structuring around the fully dissociated dimer strands was also analyzed where the H-bonding sites were exposed to the solvent. The results shown in Fig. 4B display an increase in peak intensity between the chloroform hydrogen atoms (HX) and the carbonyl oxygen atoms (O) of the dimer from 1.7 to 2.4. The effect is attributed to the newly exposed carbonyl groups of the dimer upon H-bond rupture. Nevertheless, all interactions between the solvent and the dimer models in the RDF calculations are inherently weak. Consequently, we proceeded with the analysis of the peptidomimetic β-sheets with constant velocity SMD to measure the weak, non-covalent interactions leading to mechanical stability of the simple dimer models.

4.2. Computational force spectroscopy

SMD simulations, like AFM–SMFS experiments, probe the energy barriers that determine bond strength under rapid detachment. However, because of the limits of computational resources, the timescales are 6 to 8 orders of magnitude faster, resulting in an overestimate of the rupture force. Due to the intricacy of loading-rate dependence of the rupture force, the magnitude of the forces obtained by SMD simulations cannot be compared directly with experimental data. Nevertheless, we can analyze the atomic level detail of the hydrogen bond-breaking

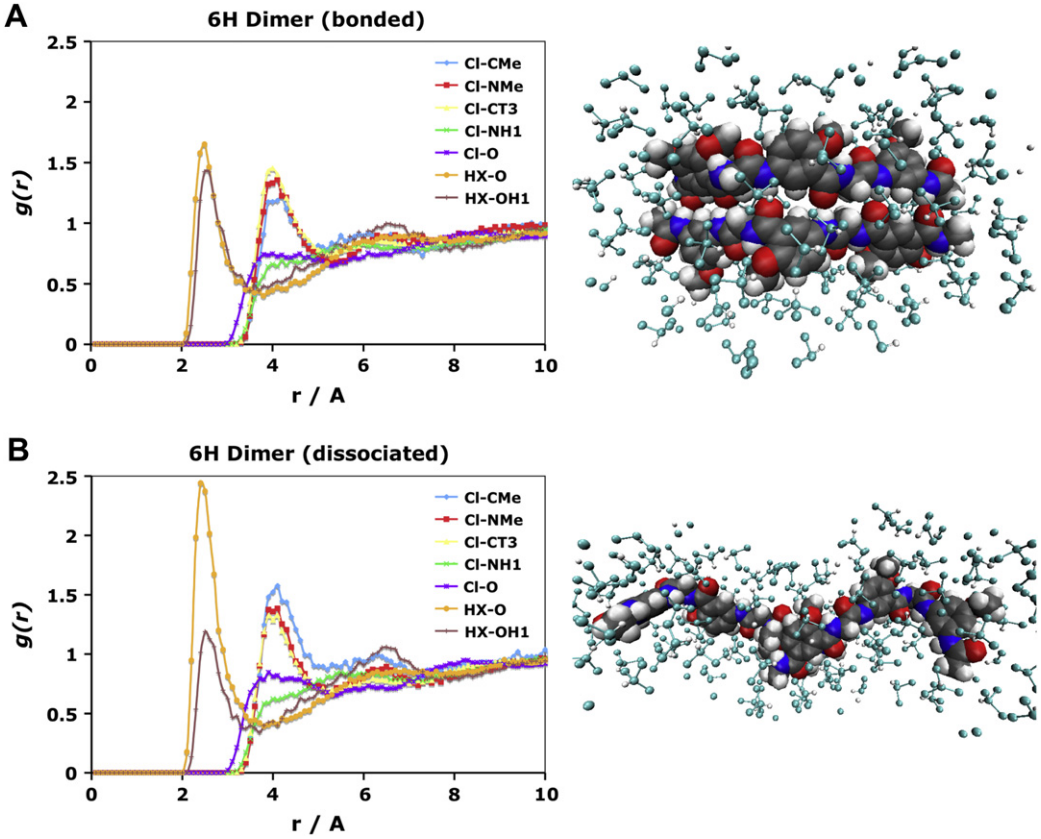

Fig. 4. Radial distribution function of chloroform around selected atom types on the 6H peptidomimetic dimer with corresponding images of the solvated model (dimer depicted by vdW representation and chloroform in CPK model). RDFs were calculated for the hydrogen and chlorine atoms of chloroform (HX and Cl, respectively) around the methyl, oxygen, and nitrogen groups of the (A) bound dimer, and (B) the fully dissociated dimer strands.

process when force is applied to the system and compare the relative force values between different dimers. The potential barrier heights reconstructed in the simulations reveal relative trends that provide insight into the reaction pathway of the rupture events.

Fig. 5 shows representative force-extension profiles with corresponding H-bond analyses obtained from constant velocity SMD at 0.01 Å/ps in chloroform as solvent. The graphs are the result of 4 averaged simulations. The force exerted by the virtual spring increases upon extension until a threshold is reached, represented by the peaks in the graphs, causing the assembly to breakdown with subsequent decrease in force. The major peaks at approximately 2.0, 3.7, and 8.0 Å extension represent the H-bond rupture event for the 4H, 6H, and 8H β-sheet mimics, respectively. The peak forces for the 4H, 6H, and 8H systems at this pulling rate are 800, 900, and 1150 pN, respectively.

For each trajectory, the pair interactions of the intermolecular hydrogen bonds were plotted over time to examine the rupture events in the force-extension profiles. The hydrogen bond rupture distance of 3.5 Å was estimated from a reported analysis of H-bonds in peptides, which ensures complete dissociation [22]. The analysis confirms the simultaneous rupture of the H-bonds as the primary event for each model. In addition, the graphs for the 6H and 8H dimers show secondary peaks at approximate extensions of 9 Å and 17 Å, respectively. Because of the increased number of hydrogen bonding sites for 6H and 8H systems, SMD simulations also showed the possibility of new combinations of H-bonds captured as the

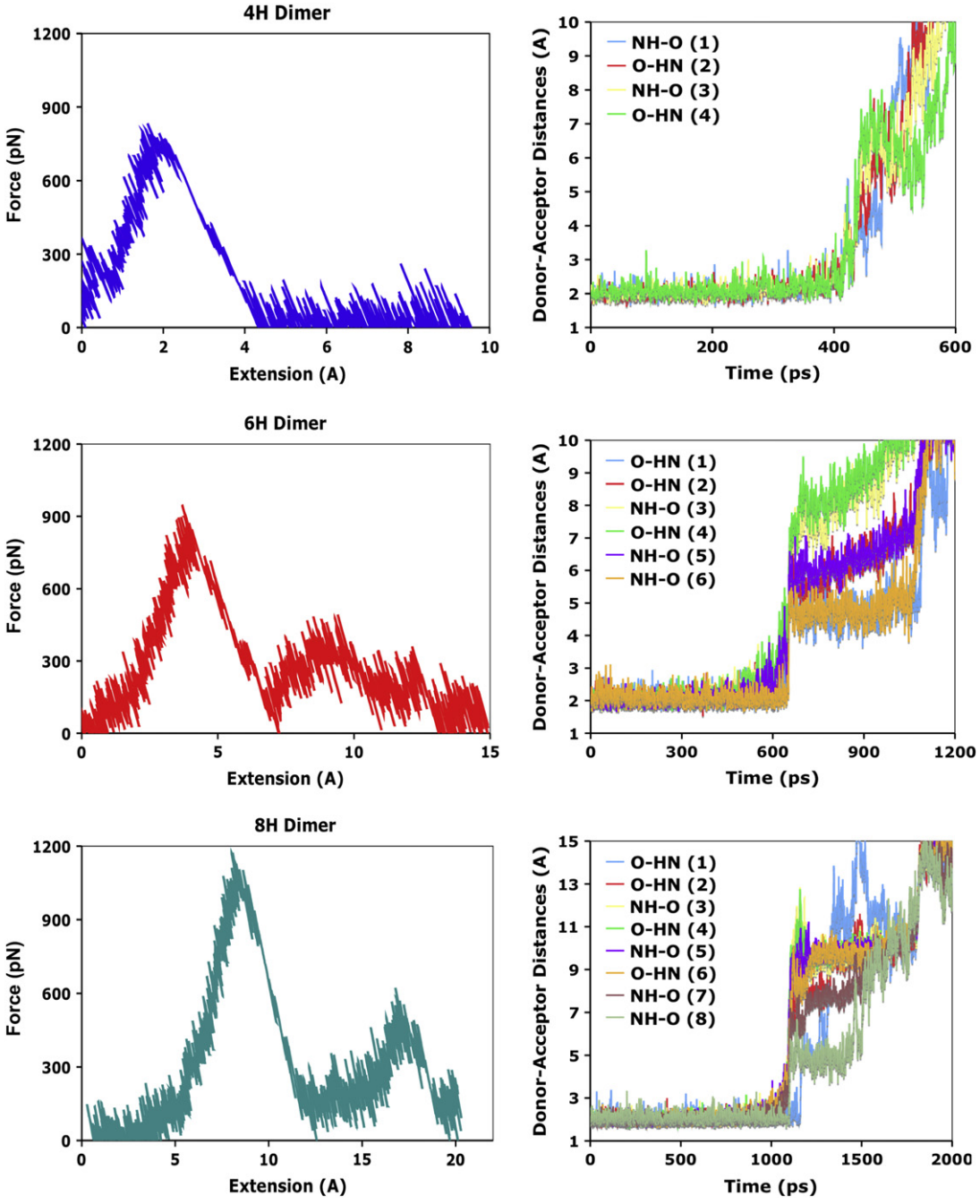

Fig. 5. SMD force-extension profiles with corresponding hydrogen bond donor–acceptor distances for the 4H, 6H, and 8H peptidomimetic β-sheets (force plots are averaged from 4 simulations at 0.01 Å/ps). Distances between interstrand hydrogen bond donors and acceptors over time course of simulations for the peptidomimetic β-sheets showing concerted rupture of all H-bonds giving rise to the major force peaks (bonds were considered ruptured at distances > 3.5 Å).

strands were pulled past each other. Fig. 6 illustrates the possible misaligned intermediates for the 6H and 8H peptidomimetic β-sheets along the unbinding trajectory stretched at a constant velocity of 0.01 Å/ps. The initial snapshot displays the alignment of the dimer strands just before rupture. This is followed by the rupture event where the strands dissociate and are pulled passed each other. Finally, in some instances, the strands form secondary interactions by forming new H-bonds. For the 6H dimer, the secondary intermediate can form 2 new H-bonds, which do not contribute much force (~370 pN). In contrast, the 8H dimer can form 4 new H-bonds that display significant mechanical stability (average of 550 pN). Note that misalignment was not captured in every simulation, but depends on the dissociation pathway; hence the average value may be decreased (see Supplementary data for force-extension profiles of individual simulations).

The calculated rupture force at 0.01 Å/ps pulling velocity for the 6H dimer (900 pN) is lower than the calculated value for titin (~1200 pN) at the same pulling rate despite the fact that the load bearing A'–G parallel sheet in titin also has 6 hydrogen bonds [5d]. This can be attributed to other secondary interactions existing in proteins that can further enhance their mechanical stability. In addition to hydrogen bonding, a protein in an aqueous environment experiences hydrophobic core packing, salt-bridge interactions, and side chain contacts which also significantly contribute to the overall mechanical stability of a protein, leading to a higher force at rupture. The mechanical unfolding trajectory of our dimer models in organic solvent illustrates a much simpler mechanism of bond rupture that is uncomplicated by secondary interactions and solvent effects seen in protein unfolding. The peptidomimetic β-sheet models do not contain such secondary interactions; therefore, the calculated rupture force is only due to the cooperative effect of the multiple hydrogen bonds breaking. Nevertheless, the mechanical stability of our simple dimers in organic solvent is still relatively high, and the incorporation of such programmed units into polymers should lead to substantial enhancement of mechanical properties. It is noted that in bulk solid state of polymers, other intramolecular and intermolecular secondary interactions, including π–π stacking, dipole–dipole, and van der Waal interactions, should further enhance their mechanical properties.

To examine the rate-dependence of dimer dissociation, SMD simulations were performed at various pulling rates: 0.01, 0.1, 0.5, and 1.0 Å/ps. Because hydrogen bond rupture is a dynamic process, our simulations should exemplify the expected behavior of the system under nonequilibrium conditions. According to the theoretical Bell–Evans model for bond dynamics, the strength of bonds is inherently dependent on the rate of the applied force [2]. Consequently, an increase in pulling rate should lead to an increase in rupture force based on the decreased lifetime of the bonds. As shown in Fig. 7, the forces for dimer dissociation were rate-dependent, demonstrated by the increase in force with increased pulling rate (the resulting force curves are averaged from 4 simulations per pulling speed). Additionally, the simulations exhibit an increase in rupture force as the number of hydrogen bonds was increased from 4 to 8, as expected. These observations lend support to the validity of our approach in using a simplified model of our peptidomimetic β-sheets to analyze mechanical stability.

4.3. AFM-based force spectroscopy

In order to validate the computational results, we synthesized the 4H, 6H, and 8H strands and carried out AFM–SMFS experiments on the peptidomimetic β-sheets following reported procedures in toluene [3–7,24,25]. The position for the pulling atom on the terminal phenyl ring was changed from *ortho* position in 4H strand to *meta* position for 6H and 8H strands to avoid undesirable lone pair repulsion between 2 adjacent O atoms. In our initial design, we observed structural instability for the analogous 6H and 8H strands having the pulling atoms on *ortho* position of the terminal phenyl rings. Although our simulations were performed using chloroform as solvent, toluene was used in the force spectroscopy studies due to its higher boiling point and decreased evaporation levels over the duration of the experiments. In addition, because chloroform did not display any considerable participation in the rupture events, it was not expected that switching to toluene would have any significant effect. Disulfide-terminated polyethylene glycol (PEG) monolayers were deposited onto gold-coated silicon wafers and gold-coated silicon nitride AFM cantilevers. PEG monolayers have been shown to minimize nonspecific interactions arising from surface–surface contact, and the known mechanical properties of PEG aid in determining single-molecule stretching events. The resulting PEG monolayers were functionalized by coupling the terminal alcohol with a series of isocyanate-terminated β-sheet mimics. The monolayers were confirmed by polarization modulation FTIR reflection–adsorption spectroscopy [26]. As the AFM tip and functionalized surface are brought into close proximity, dimerization can occur. Based on the lifetime of these complexes

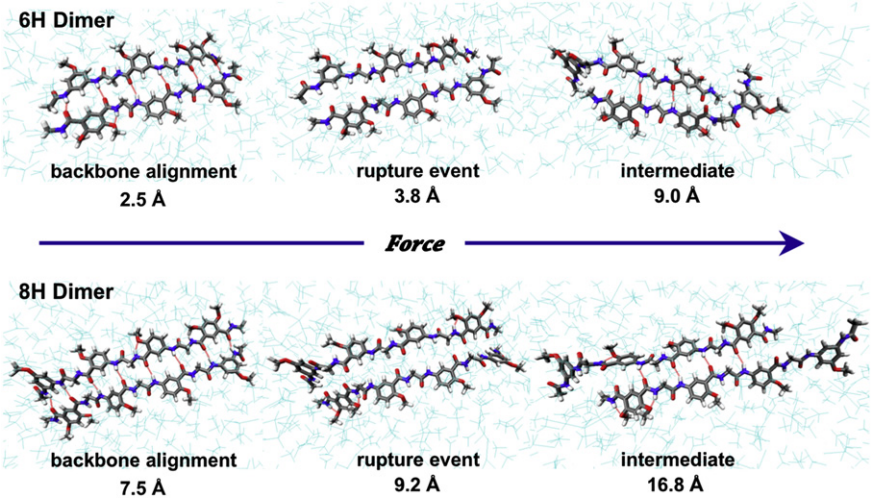

Fig. 6. SMD trajectories of the 6H (top) and 8H (bottom) peptidomimetic β-sheets illustrating the mechanism of bond rupture at 0.01 Å/ps stretching. The straightening of the backbone, rupture event, and secondary H-bonding intermediates are displayed with the corresponding extensions. (The chloroform solvent is depicted in cyan. For interpretation of the references to colour in this figure legend, the reader is referred to the web version of this article.)

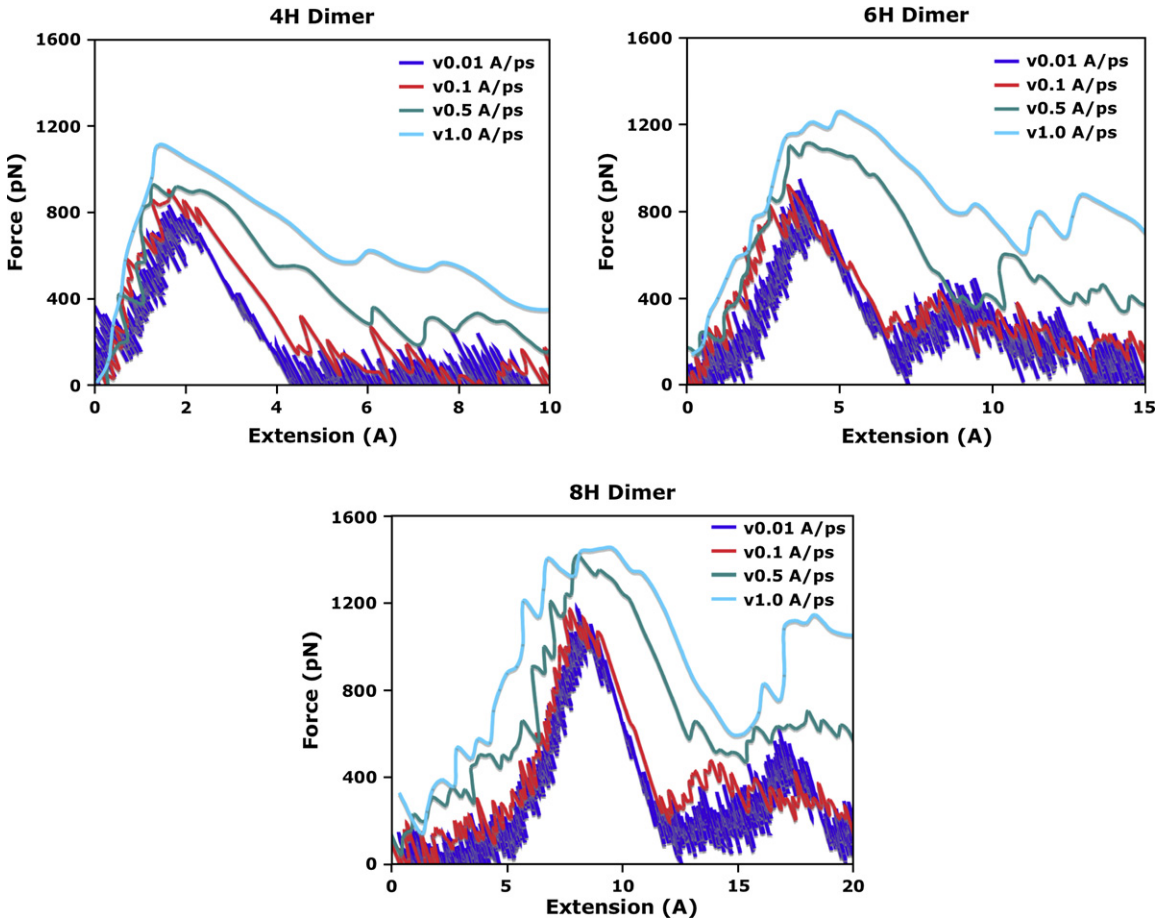

Fig. 7. SMD force curves at various pulling rates displaying the rate dependence of the peptidomimetic β-sheets. Each curve plotted is an average of 4 simulations conducted per pulling speed.

(milliseconds to seconds), H-bond rupture events can be recorded as the surfaces are pulled apart, providing the mechanical force required to break the H-bonded peptidomimetic β-sheets (Fig. 8).

SMFS data were collected with a pulling velocity of 200 nm/s using multiple cantilever probes to ensure consistency in the measurements. To ensure our recorded data represented single-chain stretching events, control experiments were performed. Pulling experiments without β-sheet modified AFM cantilevers or substrates did not show any stretching events. Similarly, β-sheet modified surfaces and only PEG modified AFM cantilevers failed to show stretching events. Only when experiments were run with β-sheet modified AFM cantilevers and substrates were single-molecule stretching events recorded. A representative force-extension curve for the 4H peptidomimetic β-sheet is shown in Fig. 9A. Only curves that could be fitted with the worm-like chain (WLC) model of single polymer chain elasticity were used in the statistical analysis. Additionally, only rupture events between 10 and 40 nm were used, with the most probable rupture events occurring at approximately 25 nm. The observed rupture events agree with the calculated contour length of the systems under study. The calculated contour lengths for the 4H, 6H and 8H systems are 24, 26, and 27 ± 1 nm, respectively. Histograms of rupture forces were fit using a Gaussian distribution which yielded most probable unfolding forces for the 4H, 6H and 8H β-sheet mimics of 75, 96 and 104 pN, respectively (Fig. 9C). The unfolding forces for these peptidomimetic dimers are weaker than the value for titin ($\sim$200 pN) measured in aqueous environment at similar pulling velocity [3]. Again, this can be attributed to other secondary interactions, such as hydrophobic core packing, salt-bridge interactions, and side chain contacts, existing in titin that further enhance its mechanical stability. The individual forces for all three dimers were plotted against rupture length to examine the relative density distribution (Fig. 9B). The graph illustrates an increase in force from the 4H to 6H distribution, whereas the force difference between the 6H and 8H distributions is relatively small (plot shows considerable overlap in the data points for the 6H and 8H forces).

Although the absolute force values cannot be compared with simulations, it was initially expected that the 8H dimer model would result in a significant increase of the rupture force due to the additional hydrogen bonding sites. On the contrary, force spectroscopy measurements showed a relatively small increase in unfolding forces from the 6H to the 8H dimer. This result led us to consider other possible secondary interactions of the 8H dimer that may play a role during the AFM–SMFS measurements. Evidence of other possible interactions was initially observed during ^{1}H NMR experiments used to characterize the hydrogen-bonded 8H β-sheet structure. Fig. 10 shows the ^{1}H NMR spectrum of the 8H β-sheet mimic in solution. Despite high purity of the sample, the ^{1}H NMR spectrum collected in chloroform-*d* at room temperature is not well resolved, showing complex peak patterns that suggest the existence of a mixture of species. However, upon heating the solution to 50 °C, a clean, well-resolved spectrum was obtained (lower spectrum). These observations suggest that the extended length of the 8H β-sheet mimic may facilitate formation of mismatched dimers, leading to complex ^{1}H NMR patterns at room temperature, which is the temperature used in AFM experiments. At elevated temperatures, these weak secondary interactions can be disrupted to leave only the fully aligned and thermodynamically most stable dimer in

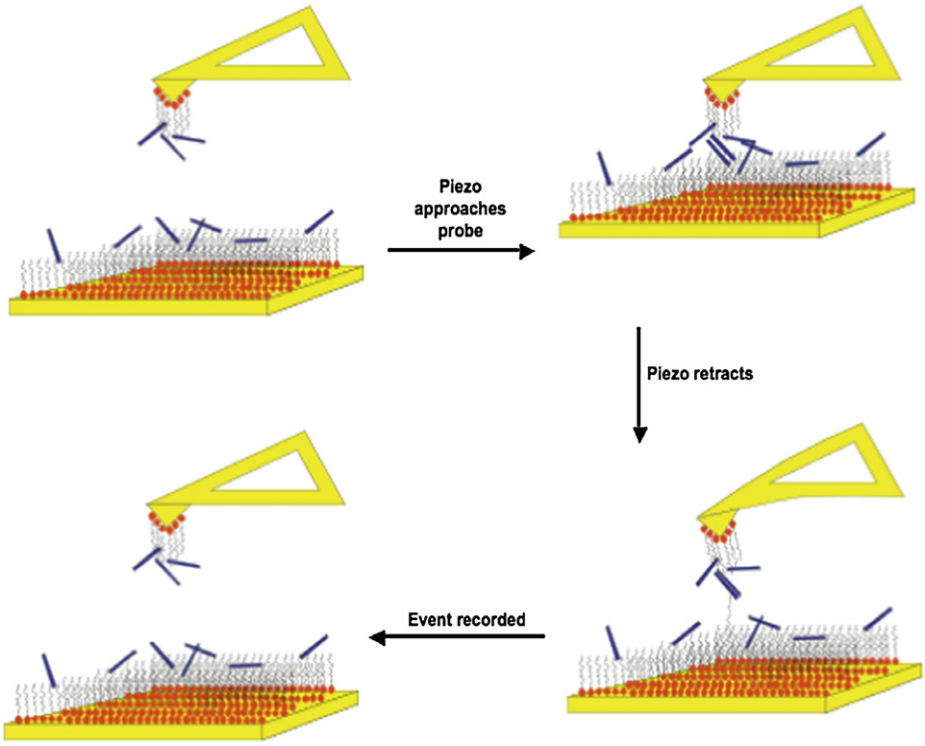

Fig. 8. Schematic representation of forced bond dissociation using AFM–SMFS of peptidomimetic β-sheets; the substrate and the probe are functionalized with monolayers of the respective monomers that can self-assemble as the piezo stage approaches the cantilever.

solution. The relatively high chemical shift values for the amide protons at 50 °C, along with NOESY data, confirm that the strands exist as perfect dimers under these conditions. On the contrary, the smaller 4H and 6H models do form well-resolved H-bonded dimers at room temperature.

4.4. Computational interpretation of AFM–SMFS

To provide potential insight into the unexpected mechanical behavior of the 8H dimer system, we carried out SMD simulations to identify other likely intermediates that may contribute to the

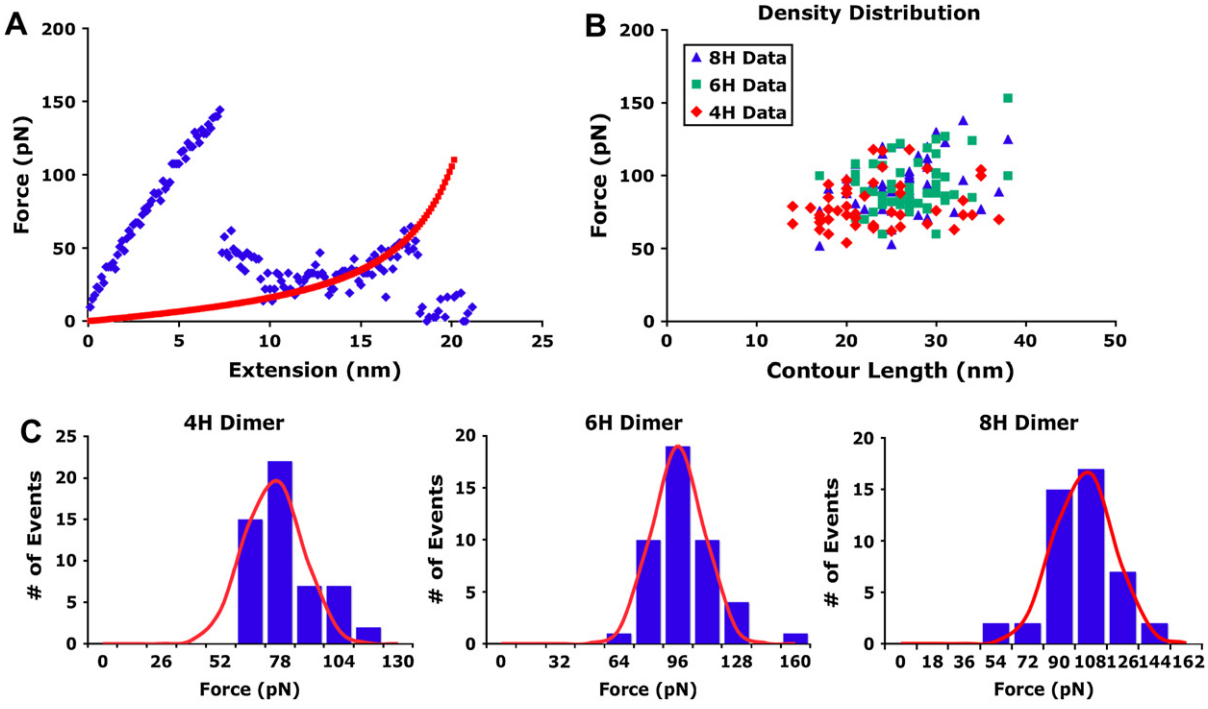

Fig. 9. (A) Representative force-extension curve for the 4H peptidomimetic β-sheet measured by AFM at 200 nm/s in toluene (red solid line is WLC fit); (B) density plot of force versus contour length for all 3 dimers; (C) histogram of rupture forces for the peptidomimetic β-sheets (Gaussian fit shown as red line. For interpretation of the references to colour in this figure legend, the reader is referred to the web version of this article.)

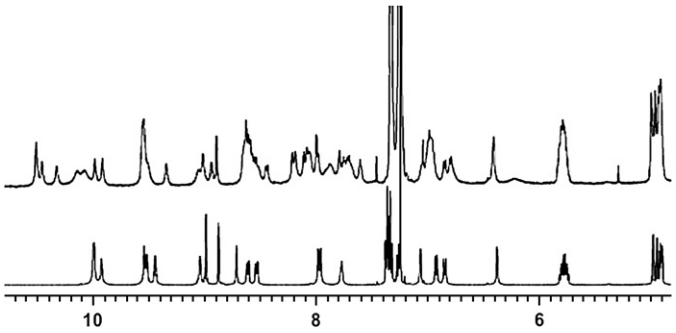

Fig. 10. Top: ^{1}H NMR spectra of the 8H peptidomimetic β-sheet mimic in chloroform-*d* at room temperature displaying broad, unresolved peaks. Bottom: ^{1}H NMR spectrum heated to 50 °C showing well-defined peaks in the amide region.

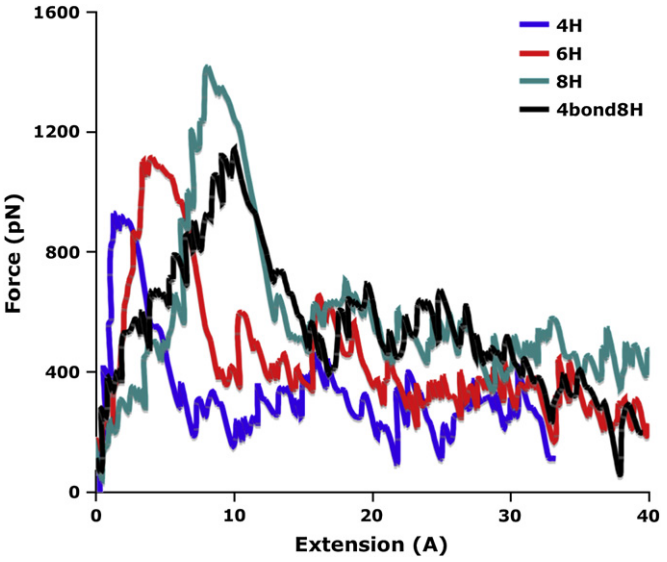

Fig. 11. SMD force-extension profile of the 8H misaligned intermediate (4bond8H) versus the 4H and 6H peptidomimetic β-sheets illustrating the similarity in mechanical stability and complementing experimental observations. The simulations plotted were performed at 0.5 Å/ps.

lower than expected mechanical properties of the dimer in solution. As shown in the force-extension profile in Fig. 5 and the trajectories in Fig. 6, the unbinding pathways for the 6H and 8H β-sheets show a secondary intermediate with evident resistance to bond rupture. Although the dimers were designed to minimize secondary interactions, it is not possible to avoid all misalignments. While these structures became apparent in simulations, the experimental limitation of the AFM resolution prevented detection of the less than 1 nm separation between primary and secondary events, consistently showing a single peak for the bond rupture. To test the mechanical stability of the 4 H-bonded mismatched intermediate for the 8H β-sheet mimic, the structure was further minimized and equilibrated for 1 ns to obtain the lowest energy conformer. The extension of the dimer was offset by 17 Å to set the intermediate structure as the starting point for stretching. SMD simulations performed on the 8H-mismatched structure exhibited forces similar to those of the 6H dimer (Fig. 11). These observations lend support to other possible misaligned structures contributing to the lower than expected increase in rupture force for the 8H dimer, and illustrate the power of combining simulations with experiment to probe these interactions for materials design. Given the relatively large size and conformational flexibility of the 8H β-sheet mimic, and low solubility in toluene at room temperature, it is possible that the misaligned intermediate could be the dominant dimerization species during the kinetic process of AFM pulling experiments. These limitations did not exist for the smaller and more soluble 4H and 6H β-sheet mimics, leading to facile formation of the correctly matched dimers.

Interestingly, although the 8H mismatched intermediate structure only forms 4 hydrogen bonds, the simulated rupture force is significantly higher than the force for the 4H system (Fig. 11). Atomic level analysis of the unfolding pathway reveals that the pulling trajectory with respect to the H-bonded plane of the dimers is directly correlated to the observed rupture force. Fig. 12 illustrates the pulling geometry of the peptidomimetic β-sheets with corresponding angles of bond rupture. Analysis of the dissociation mechanism reveals that the pulling vector for the 4H dimer has a smaller angle ($\sim 35^{\circ}$) with respect to the direction of bond rupture than that observed for the 8H intermediate, which is approximately 50°. Since the major event for both structures involves simultaneous rupture of the 4 interstrand H-bonds, application of the extended Bell model predicts that increasing the angle of the applied force decreases its effect on the mechanical energy barrier, resulting in an observed increase in rupture force ($F_1(v) \cdot \cos\theta_1 = F_2(v) \cdot \cos\theta_2$, where $\theta_2 > \theta_1$) [23]. Using the force and rupture angle of the 4H dimer as the reference point, the 8H-mismatched intermediate is predicted to have a rupture force of 96 pN, closely correlating to the observed AFM force of 104 pN.

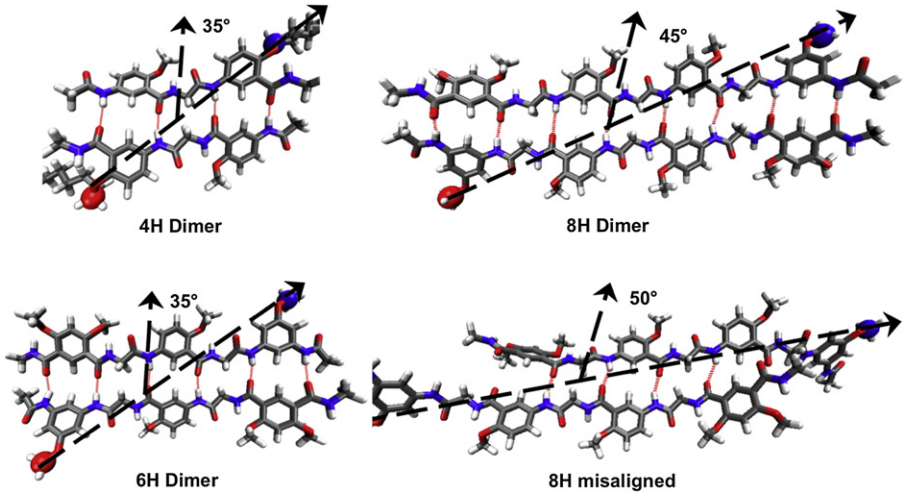

Fig. 12. Force vector applied to the peptidomimetic β-sheets shown with corresponding angles of the direction of H-bond rupture.

Furthermore, we can extend this analysis to estimate the force transferred to each hydrogen bond in the dimer models, since the interactions are simplified compared with proteins. Without the complication of other secondary interactions as existing in proteins, in principle, the rupture force should only depend upon the number of hydrogen bonds and the rupture angle. In the case of the 4H and 6H peptidomimetic β-sheets, the number of H-bonds is increased by 2, but the rupture angles are identical (35°) as a result of the modification in pulling atom positions on the benzene ring. For the mismatched 8H dimer, the number of effective hydrogen bonds is equivalent to the one in the 4H dimer, but the rupture angle is larger (50°). If we assume the forces are evenly distributed to each hydrogen bond and only the force component parallel to the hydrogen bonding direction (i.e., $F\cos(\theta)$) will cause rupture of hydrogen bonds, the force component transferred to each hydrogen bond is estimated to be 15 ± 2 pN for the 3 systems.

5. Conclusion

In this article we applied steered molecular dynamics simulations and AFM-based SMFS to investigate the molecular mechanisms involved in dissociating a series of peptidomimetic β-sheets under an applied force. Combining simulation and experiment provided a unique approach to study the behavior of the nanostructures in organic solvent, with greater insight into the chemical design for mechanically strong modules. The dimers were modeled in explicit chloroform, and the effects of solvation were analyzed to reveal minimal interaction with the dimers (Fig. 4). Steered molecular dynamics calculations established the expected unbinding forces for the 4H and 6H dimer models, corroborating experimental results (Figs. 5 and 9), and predicted the forces for the well-aligned 8H dimer. Additionally, the trajectories of the model systems illustrated the possibility of secondary interactions showing significant mechanical stability. These observations allowed identification of an 8H mismatched intermediate as a probable structure present during experimental studies, giving rise to a lower force for this system than expected (Fig. 11). Finally, comparison of the resulting force and pulling geometry of the 8H mismatched intermediate provided support for the structure as the kinetic product in experimental force studies (Fig. 12).

Having validated the computational methods with experiments, this technique provides an effective means of probing mechanical behavior of novel nanostructures prior to synthesis. Despite its simplicity, the predictive potential of this approach can be used to guide further design of modular polymers having advanced mechanical properties through programming weak, non-covalent molecular forces. Because of the complex hierarchical organization of natural mechanical materials, it remains a challenge to engineer biomimetic materials that equal the exceptional combined toughness and elasticity. Application of single-molecule methods and molecular dynamics simulations will continue to extend the knowledge of nanoscale organization for bottom-up development of synthetic materials.

Acknowledgements

We are thankful for the financial support from the National Institutes of Health (R01EB004936) and the Department of Energy (DE-FG02-04ER46162). We also thank Dr. Douglas Tobias and Neelanjana Sengupta (University of California, Irvine) for helpful discussions and development of chloroform parameters for use in CHARMM force field.

Appendix. Supplementary data

Synthesis and characterization of peptidomimetic β-sheets **1**–**3**; AFM–SMFS analysis of the peptidomimetic β-sheets; SMD force-extension profiles for individual dimer simulations.

Supplementary data associated with this article can be found in the online version, at doi:10.1016/j.polymer.2008.06.047.

References

[1] Binning G, Quate CF, Gerber G. Phys Rev Lett 1986;56:930–3.
[2] (a) Janshoff A, Neitzert M, Oberdorfer Y, Fuchs H. Angew Chem Int Ed 2000;39:3213–37;
(b) Zhang WK, Zhang X. Prog Polym Sci 2003;28:1271–95;
(c) Liu CJ, Shi WQ, Cui SX, Wang ZQ, Zhang X. Curr Opin Solid State Mater Sci 2005;9:140–8.
[3] Rief M, Gautel M, Oesterhelt F, Fernandez JM, Gaub H. Science 1997;276:1109–12.
[4] Carrion-Vazquez M, Marszalek PE, Oberhauser AF, Fernandez JM. Proc Natl Acad Sci U S A 1999;96:11288–92.
[5] (a) Lu H, Isralewitz B, Krammer A, Vogel V, Schulten K. Biophys J 1998;75:662–71;
(b) Marszalek PE, Lu H, Li H, Carrion-Vazquez M, Oberhauser AF, Schulten K, et al. Nature 1999;402:100–3;
(c) Lu H, Schulten K. Biophys J 2000;79:51–65;
(d) Gao M, Lu H, Schulten K. J Muscle Res Cell Motil 2002;23:513–21.
[6] Schulten K, Lu H. Proteins Struct Funct Genet 1999;35:453–63.
[7] Li H, Carrion-Vazquez M, Oberhauser AF, Marszalek PE, Fernandez JM. Nature 2000;7:1117–20.
[8] Guan Z, Roland JT, Bai JZ, Ma SX, McIntire TM, Nguyen M. J Am Chem Soc 2004;126:2058–65.
[9] Roland JT, Guan Z. J Am Chem Soc 2004;126:14328–9.
[10] Kushner AM, Gabuchian V, Johnson EG, Guan Z. J Am Chem Soc 2007;129:14110–1.
[11] Isralewitz B, Gao M, Schulten K. Curr Opin Struct Biol 2001;11:224–30.
[12] Ng SP, Rounsevell RWS, Steward A, Geierhass CD, Williams PM, Paci E, et al. J Mol Biol 2005;350:776–89.
[13] Kim T, Rhee A, Yip CM. J Am Chem Soc 2006;128:5330–1.
[14] Gong B. Synlett 2001;5:582–9 and references cited therein.
[15] Phillips JC, Braun R, Wang W, Gumbart J, Tajkhorshid E, Villa E, et al. J Comput Chem 2005;26:1781–802.
[16] (a) Brooks BR, Bruccoleri RE, Olafson BD, States DJ, Swaminathan S, Karplus M. J Comput Chem 1983;4:187–217;
(b) MacKerell Jr AD, Brooks B, Brooks III CL, Nilsson L, Roux B, Won Y, et al. In: Schleyer PVR, editor. The encyclopedia of computational chemistry, vol. 1. Chichester, UK: John Wiley and Sons; 1998. p. 271–7.
[17] Humphrey W, Dalke A, Schulten K. J Mol Graphics 1996;14:33–8.
[18] MacKerell, AD. Strategies for Parameter Developments. Available from <http://www.psc.edu/general/software/packages/charmm/tutorial/mackerell/PARAM_00.pdf>.
[19] Case DA, Darden TA, Cheatham III TE, Simmerling CL, Wang J, Duke RE, et al. AMBER 8. San Francisco: University of California; 2004.
[20] (a) Pabon G, Amzel M. Biophys J 2006;91:467–72;
(b) Dougan L, Feng G, Lu H, Fernandez JM. Proc Natl Acad Sci U S A 2008;105:3185–90.
[21] Yu I, Iwata K, Ueda K, Nakayama H. Bull Chem Soc Jpn 2003;76:2285–92.
[22] Sheu SY, Yang DY, Selzle HL, Schlag EW. Proc Natl Acad Sci U S A 2003;100:12683–7.
[23] (a) Evans E, Ritchie K. Biophys J 1997;72:1541–55;
(b) Evans E. Annu Rev Biophys Biomol Struct 2001;30:105–28.
[24] Hinterdorfer P, Kienberger F, Raab A, Gruber HJ, Baumgartner W, Kada G, et al. Single Mol 2000;1:99–103.
[25] Zou S, Schonherr H, Vancso GJ. Angew Chem Int Ed 2005;44:956–9.
[26] Roland, JT. Modular domain structure: a biomimetic strategy for advanced polymeric materials. PhD Dissertation. University of California, Irvine; 2006.